Mon. Not. R. Astron. Soc. **261**, 855–864 (1993)

The density structure of a galaxy influenced by a massive companion

P. M. S. Namboodiri and R. K. Kochhar
Indian Institute of Astrophysics, Bangalore 560034, India

Accepted 1992 October 8. Received 1992 September 10; in original form 1992 April 22

ABSTRACT

The tidal influence of a massive galaxy on a non-rotating spherical companion is studied using numerical simulations. The simulations use various values of mass ratio and velocity of collision while the pericentric distance is kept constant. The half-mass radius of the final equilibrium system remains almost the same as that of the initial system with which the simulations started. The central region becomes more compact and the outer region shows expansion. Maximum tidal distension is observed when galaxies undergo collision on parabolic orbits. The surface density profile of the remnant follows an $r^{1/4}$ law up to $r=4R_h$, where R_h is the half-mass radius. The profile shows evidence for a tendency to develop bulges in the outer parts in encounters in which the masses of the stellar systems are comparable.

Key words: methods: numerical – celestial mechanics, stellar dynamics – galaxies: interactions – galaxies: kinematics and dynamics – galaxies: structure.

1 INTRODUCTION

The importance of tidal effects on shaping the structure of a galaxy has been recognized for many years. Several numerical simulations have shown that a spherical galaxy is transformed into a spheroidal system during a tidal encounter (White 1978; Rao, Ramamani & Alladin 1987; Dekel, Lecar & Shaham 1980; Namboodiri & Kochhar 1990, hereafter Paper I). Two types of tidal effect are generally observed in elliptical galaxies. The first is tidal stripping in a victim galaxy which is influenced by a much larger companion. The effect of tidal force in such galaxies is to remove outer haloes, thereby reducing the size of the victim. A few compact elliptical galaxies, such as M 32, NGC 4486B and NGC 5846A, are examples of tidally stripped galaxies (Faber 1973; Nieto & Prugniel 1987). These peculiar elliptical galaxies have high surface brightness and low luminosity. Prugniel, Davoust & Nieto (1989) investigated eight close pairs of ellipticals, each involving a bright galaxy and a faint companion. Even though they noticed tidal truncation in some of the faint companions, they could not exclusively attribute this property to tidal interaction. One of the faint companions belonged to a loose pair which exhibited a regular density profile. They pointed out that correlation between compactness and tidal truncation cannot be considered as conclusive evidence for tidal interaction. However, none of their pairs showed as strong a tidal truncation as that observed in NGC 4486B.

The other effect seen in interacting galaxies of similar mass and size is tidal distension. Kormendy (1977) has shown that ellipticals with nearby companions of comparable luminosity have bright envelopes above the extrapolation of a de Vaucouleurs' law fitted to the inner parts. The envelopes are generally reduced or absent in isolated galaxies. A number of ellipticals which show luminosity excess in their outer regions when fitted with de Vaucouleurs' law have luminous companions within several galactic diameters. Kormendy interpreted this as tidal distension produced by the close passage of a large companion. The surface brightness of NGC 3379 follows an $r^{1/4}$ law in the inner parts and shows distension in the outer parts. This galaxy has two companions. Prugniel et al. (1989) observed that the profiles of the bright galaxies in their sample obeyed an $r^{1/4}$ law. The outer parts were tidally distended even though the amplitude of distension did not correlate well with the presence of close neighbours. Tidal distension has been seen in many numerical simulations (Gutowski & Larson 1976; van Albada & van Gorkom 1977; Wielen 1977; White 1978; Miller & Smith 1980; Aguilar & White 1986; Navarro 1990). White (1978, 1979) considered the merger of two similar galaxies and showed that the spatial density profile of the merger remnants follows a power law with exponent near -3. However, the surface density profiles were reasonably described by de Vaucouleurs' formula. Merger remnants showed higher central concentration, whereas the outer parts showed expansion. The remnant of parabolically colliding systems produced the most central concentration, whereas no central concentration was produced in cases where the initial relative orbit was circular. Aguilar & White (1986) performed numerical simulations of non-rotating

spherical galaxies whose initial density profiles were given by de Vaucouleurs and King models. They showed that in both cases the remnant obeyed an $r^{1/4}$ density profile within a few effective radii and the outermost parts obeyed a power law with exponent ≈ -3. The merging simulations of Navarro (1989, 1990) involving equal-mass galaxies also demonstrated the robustness of an $r^{1/4}$ law in describing the density profile of the merger remnant. Deviations from an $r^{1/4}$ law appeared in the form of a *bump* that was produced in the outer regions. The *bump* decayed in the local dynamical time-scale. McGlynn (1990) studied the remnants of strong tidal interaction in which the victim galaxy was less massive than the companion. The simulations in which the victim survived showed a density profile $\rho \propto r^{-4}$. He compared a sample of ellipticals that showed signs of tidal interaction and found good agreement with his simulations. Whatever the nature of the interaction, it apparently leads to a remnant with a typical density profile. This density profile can be reasonably represented by de Vaucouleurs' law that is characteristic of ellipticals and bulges of spiral galaxies.

Most of the earlier simulations concentrated on merging phenomena in which the components are assumed to have equal mass. The aim of the present paper is to study the evolution of the density structure of a small galaxy influenced by a large companion. Our model considers the mass ratio between the primary and secondary, M_1/M, in the range 2 to 10^3. This case is important because, in such an encounter, the less massive galaxy is subjected to maximum tidal effects. McGlynn (1990) used mass ratios 10^2 and 10^6 and his models were heavily, centrally concentrated King models which resulted in a mass loss as high as 50 per cent. On the other hand, Aguilar & White (1986) studied collisions of galaxies of comparable mass in which the final density profiles showed extension in the outer parts. Our work essentially falls between the above two cases with our models being less centrally concentrated than McGlynn's. Our simulations use a constant pericentric distance p, satisfying $p \simeq 3R$, where R is the size of the satellite. The outer parts of the smaller galaxy show tidal distension after an encounter and the subsequent density profile can be fitted by an $r^{1/4}$ law over a large range in radius containing 90 per cent of its mass.

The simulations use a limited set of collision parameters in which the effect of massive haloes is ignored. Several studies have shown the existence of a drag force on satellite stellar systems. However, the orbital decay is predicted to be very slow if the ratio of the orbital radius to the size of the satellite is larger than about two (Tremaine & Weinberg 1984), as is actually the case in all our models. A crude estimate for the dynamical friction time is given by Gelato, Chernoff & Wasserman (1992). This makes use of Chandrasekhar's (1943) dynamical friction formula and expects the satellite to be considered as a Plummer model. The orbital period of a satellite of mass M orbiting a heavy body of mass $M_1 \gg M$ with relative velocity v at radius R is $t_{\rm orb} = 2\pi R/v$. The decay time $t_{\rm ch}$ is given by

$$\frac{t_{\rm ch}}{t_{\rm orb}} = \frac{1}{t_{\rm orb}} \frac{v}{|{\rm d}v/{\rm d}t|} = \frac{1}{8\pi^2 \ln \Lambda} \left(\frac{M_1}{M}\right)\left(\frac{M_1}{\rho_{<v} R^3}\right). \quad (1)$$

Here $\rho_{<v}$ is the mass density in the background particles with speed less than v and Λ is the ratio of the maximum to the minimum impact parameter. We take $\Lambda = 2$ and $\rho_{<v} \simeq \rho$ and assume that

$$\frac{M_1}{\rho R^3} = \frac{4\pi}{3}\left(\frac{r_{\rm c}}{R}\right)^3 \left[1 + \frac{R^2}{r_{\rm c}^2}\right]^{5/2}. \quad (2)$$

Substituting (2) in (1), we get

$$\frac{t_{\rm ch}}{t_{\rm orb}} \simeq \frac{R^2/r_{\rm c}^2}{6\pi \ln \Lambda}\left(\frac{M_1}{M}\right)\left[1 + \frac{r_{\rm c}^2}{R^2}\right]^{5/2}. \quad (3)$$

The computed orbital decay times are given in column 11 of Table 2, where we have used $R_{\rm h} = 1.3 r_{\rm c}$. It can be seen that the effect of dynamical friction is negligible in our models.

Our numerical simulations are described in Section 2. The results are presented and discussed in Section 3. The conclusions are given in Section 4.

2 THE SIMULATIONS

2.1 Initial conditions

Our model consists of two galaxies of masses M and M_1 with $M < M_1$. The more massive galaxy, called the primary or the perturber, is treated as a mass point. The less massive test galaxy or satellite is modelled as a spherical cluster containing 250, 500 or 1000 equal-mass points. We use a dimensionless system of units in which $G = 1$. The simulations with $N = 250$ are denoted as A models; those with $N = 500$, B models and those with $N = 1000$, C models. In A models the particles are initially distributed within a sphere of radius $R = 20$ units and in B and C models the radius of the initial sphere is $R = 10$ units. The particles are distributed using a random number generation technique in such a way that the initial mass distribution follows the law $M(r) \propto r$. Each particle is initially given a velocity equal to the circular velocity appropriate to its position and the directions of the velocity vectors are chosen randomly. A softened potential is used with the softening parameter $\epsilon = 0.1R$ in A models and $\epsilon = 0.05R$ in B and C models. In each model the test galaxy is evolved for about eight crossing times to obtain a dynamically stable system. Aarseth's NBODY2 code is used for numerical integration. The evolved systems, called the standard models, are very close to virial equilibrium, are almost spherical in size, and possess no net angular momentum – no particles escape from them during this initial evolution. They contain 90 per cent of the mass within about $3R_{\rm h}$. These standard models are used for subsequent encounters. The parameters of the standard models are given in Table 1.

Table 1. Parameters of the standard models.

Model	q	R_h	$R_{0.9}$	R	R_{rms}	V_{rms}	V_{disp}
A	0.44	6.55	18.62	36.62	10.81	3.42	1.45
B	0.45	2.29	7.00	18.97	5.36	7.72	3.41
C	0.45	2.27	7.42	16.25	5.28	10.91	4.88

Note: $q = T/W$, where T and W are the total kinetic and potential energies; $R_{\rm h}$ is the half-mass radius; $R_{0.9}$ is the radius containing 90 per cent mass; $R_{\rm rms}$ and $V_{\rm rms}$ are respectively the root mean square radius and velocity; $V_{\rm dsp}$ is the velocity dispersion.

2.2 Collision parameters

The standard models described above are now perturbed by a massive point-mass galaxy. Ideally one should model the perturber also as a cluster of particles. Since we are interested in the dynamics of the satellite, which is likely to suffer maximum damage during an encounter, we consider the assumption of a point-mass perturber to be reasonable.

The important parameters in a galaxy collision are the impact parameter, the velocity of collision and the mass ratio of the stellar systems. We have performed a series of simulations for a wide range of values of mass ratio and velocity of collision. We consider various models in which the initial relative orbit of the perturber is hyperbolic (models H, HB, HC), parabolic (models P, PB, PC), elliptic (models E, EB, EC) and circular (model C). The sudden introduction of the perturber is likely to cause instabilities in the satellite which can be minimized by choosing the initial separation r_0 between the galaxies to be appreciably larger than their sizes. The initial separation $r_0 = kp$ where $k = 3$ and 2 for H and P models. The simulations are continued until the perturber reaches a distance where the tidal effects are negligible. For the bound orbit encounters, the perturber is placed at the apocentre in the orbit and the evolution followed for one complete orbit, except in model EA. In model EA only half the orbit on either side of the pericentric distance is considered. The orbits of the perturber in models HB, HC, PB, PC, EB and EC are shown in Fig. 1. Fig. 1(a) represents the orbits in models HB and HC, Fig. 1(b) those of models PB and PC, and Fig. 1(c) those of models EB and EC. The inverted triangle represents models HB, PB and EB and the filled diamond represents models HC, PC and EC. The distance of closest approach in A model is $p = 100$ and in B and C models $p = 60$. The eccentricity for initial H model is $e = 2$ and for E model $e = 0.5$. The XY plane is the orbital plane with the X-axis pointing in the direction of closest approach. The various collision parameters are given in Table 2.

3 NUMERICAL RESULTS

3.1 Analysis of numerical results

The results of the simulations at selected times are analysed with respect to the centre of mass of the satellite, which is computed in the following manner. The centre of mass of all particles in the satellite is computed first and particles with positive energy with respect to this centre of mass are identified as escapers. The centre of mass of the remaining particles is again evaluated and escapers with respect to this new origin are removed next. This process is continued until there are no more escapers. This gives the remnant bound system. We have considered those remnants in which the mass loss is less than nearly 30 per cent. It has been shown earlier that a satellite galaxy suffers considerable damage if it loses more than 30–40 per cent of its mass during an encounter. This condition seems to be satisfied if the fractional change in energy, $\Delta U/|U|$, where U is the unperturbed total energy and ΔU is its change, is greater than two. Both these conditions are satisfied in all our models. The values of $\Delta U/|U|$ and the mass loss $\Delta M/M$ are given in columns 3 and 4 respectively of Table 2.

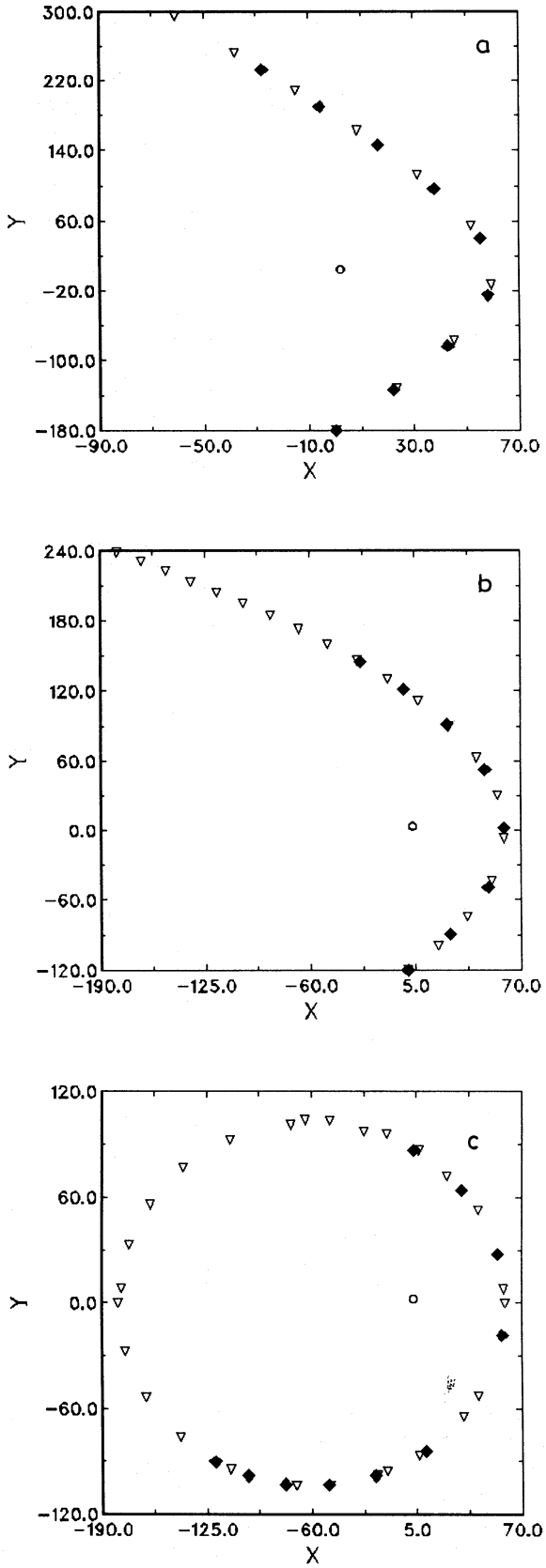

Figure 1. The relative orbits of the perturber in B and C models; the inverted triangle represents B models and the filled diamond represents C models. (a) Models HB and HC; (b) models PB and PC; (c) models EB and EC.

Table 2. Collision parameters and results.

1	2	3	4	5	6	7	8	9	10	11
Model	$\frac{M_1}{M}$	$\frac{\Delta U}{\lvert U\rvert}$	$\frac{\Delta M}{M}$	f	λ	q	r_e	-log$I(0)$	$\frac{t}{t_{orb}}$	$\frac{t_{ch}}{t_{orb}}$
INT						0.44	6.183	2.191		
H2	593.1	0.576	0.316	0.42	0.05	0.45	5.425	2.277	2.4	2513
H3	333.3	0.450	0.260	0.12	0.02	0.41	6.372	2.236	2.7	1412
H4	166.7	0.265	0.148	0.05	0.04	0.43	7.352	2.199	3.7	706
P4	166.7	0.403	0.272	0.34	0.04	0.43	6.742	2.171	1.5	706
P5	83.3	0.209	0.124	0.29	0.03	0.40	6.098	2.283	2.1	353
P6	41.7	0.131	0.068	0.29	0.04	0.41	7.215	2.172	2.1	176
P7	20.8	0.037	0.024	0.05	0.01	0.43	6.294	2.162	2.6	88
P8	10.4	0.024	0.008	0.11	0.02	0.42	5.967	2.232	2.6	44
P10	2.6	0.003	0.000	0.15	0.01	0.45	6.604	2.174	4.5	11
E5	83.3	0.290	0.236	0.13	0.03	0.43	6.464	2.122	1.4	353
E6	41.7	0.168	0.140	0.31	0.02	0.39	5.990	2.177	3.6	176
E7	20.8	0.089	0.076	0.28	0.02	0.41	6.325	2.152	5.2	88
E8	10.4	0.058	0.048	0 70	0 03	0.44	7.617	2.273	7.1	44
E10	2.6	0.018	0.004	0.88	0.02	0.41	8.741	2.413	12.5	11
C7	20.8	0.196	0.172	0.28	0.02	0.43	5.703	2.226	1.1	88
C8	10.4	0.093	0.084	0.33	0.03	0.41	5.814	2.213	1.4	44
C10	2.6	0.024	0.016	0.34	0.02	0.44	6.670	2.169	2.5	11
INTB						0.45	5.586	2.017		
HB	20.8	0.005	0.004	0.33	0.01	0.45	7.744	2.219	6.7	189
PB	20.8	0.017	0.022	0.14	0.01	0.47	5.766	2.072	4.9	189
EB	20.8	0.059	0.068	0.41	0.02	0.47	7.726	2.138	6.3	189
INTC						0.45	5.292	2.047		
HC	20.8	0.005	0.003	0.05	0.01	0.46	6.098	2.172	6.4	142
PC	20.8	0.016	0.003	0.08	0.01	0.46	5.998	2.192	3.0	142
EC	20.8	0.037	0.030	0.15	0.02	0.46	5.586	2.161	2.8	142

Notes: (1) model identification (INT represents initial A model, INTB initial B model, INTC initial C model); (2) mass ratio; (3) fractional change in energy of bound system; (4) fractional mass loss; (5) flattening parameter f; (6) spin parameter λ; (7) virial coefficient $q = T/W$, T and W being total kinetic and potential energies; (8) and (9) values determined by least-squares fit to an $r^{1/4}$ law; (10) simulation time in units of orbital time; (11) orbital decay time in units of orbital time.

Statistical fluctuations can be important when the number of particles in the simulations is small. In order to assess the significance of these fluctuations and to obtain representative values for each model, one should perform the simulations with several seeds for generating random numbers. In particular we have performed 13 simulations for model P7 ($N=250$) with different seeds for random number generation. We note from these simulations that deviations in the derived quantities are small; e.g., the virial coefficient $q=T/W$, where T and W are the total kinetic and potential energies, has a mean value $\langle q\rangle=0.44$ with $\sigma=0.015$. Similarly, the mean relative mass loss $\langle\Delta M/M\rangle=0.0263$ with $\sigma=0.007$. These experiments show that the quantities derived from an equivalent system in which $N=250$ are expected to differ from their intrinsic values by as much as 26 per cent. These deviations are expected to be still less in B and C models, in which the number of particles has been doubled and quadrupled respectively. Neither the small number of particles nor the large softening parameter seems to have introduced artificial effects in our simulations.

The evolution of the satellite to a stable configuration after an encounter has been studied by removing the perturber

and continuing the simulation for 10 more crossing times. During this evolution the total energy, the number of escapers, the angular momentum, the virial coefficient and the dimensionless spin parameter all remained nearly constant, indicating that the perturber has gone sufficiently far that transient tidal effects have become negligible.

To get an idea of the duration of an encounter, we express the simulation time in terms of the orbital time. The initial orbital time is defined as

$$t_{\rm orb} = 2\pi \left[\frac{R^3/(1+e)^3}{GM}\right]^{1/2}. \qquad (4)$$

Here the symbols have the usual meaning. The simulation time is expressed in units of orbital time and shown in column 10 of Table 2.

3.2 General features

The evolved systems in models B and C are given in Figs 2(a)–(d). In Fig. 2(a) the upper panel represents the initial galaxy (model INTB, $N=500$) in the XY, YZ and ZX planes. The lower panel shows the same galaxy after the encounter, i.e. model HB. The upper and lower panels of Fig. 2(b) respectively show the configurations of models PB and EB after the encounter. Fig. 2(c) shows models INTC ($N=1000$) and HC respectively in the upper and lower panels and Fig. 2(d) the models PC and EC. It can be seen that the spherical galaxy is flattened towards the orbital plane, which is clearly seen in models HB and HC. The degree of flattening f is computed using the formula

$$f = 1 - \frac{2I_{33}}{(I_{11}+I_{22})}. \qquad (5)$$

Here I_{11}, I_{22} and I_{33} are the moments of inertia in the X, Y and Z directions. These quantities are given in column 5 of Table 2. These values are randomly distributed and do not show any regular trend. Flattening is one of the least stable properties of these models, as has been found by White (1978).

A non-rotating spherical galaxy acquires spin as a result of an encounter, which is measured by the dimensionless spin parameter

$$\lambda = J|U|^{1/2}/GM^{5/2}. \qquad (6)$$

Here J is the angular momentum, U the total energy and M the mass of the remnant system. These values are given in column 6 of Table 2.

3.3 The radial structure of the remnant

The radial structure of the remnant bound system is shown in Table 3. The entries in this table are the radii of the regions containing 10, 20, 30,…,90 and 100 per cent of mass and they are normalized with respect to the half-mass radius of each model. These are obtained by projecting the particles on to the orbital plane. The innermost region containing 10 per cent of the mass can be taken as a measure of central concentration. The central concentration of the remnant bound system shows an increase for collisions of galaxies which have a high mass ratio. When the masses are comparable, each shell of stars moves to a radius slightly larger than its original radius. The half-mass radius $R_{\rm h}$ is also given in Table 3. It can be clearly seen that the region containing half the mass remains nearly unaltered in all the models. In fact, expansion remains negligible for the region containing 90 per cent of the mass. However, the outermost region containing the rest of the mass shows tidal distension in all models. In Table 3 we have also given the value of the tidal radius, $R_{\rm t}$, for each model computed using King's (1962) formula: $R_{\rm t}^3 = Mp^3/(3+e)M_1$. The tidal radius lies between $R_{0.6}$ and $R_{0.7}$ in H2 and H3 of model A. It is shifted to the region between $R_{0.7}$ and $R_{0.8}$ in H4, P4 and P5. In all other models (including those of categories B and C) the tidal radius lies beyond $R_{0.9}$. Thus King's formula generally underestimates the tidal radius. It may be pointed out that King's formula can be used for stellar systems situated at the centre of a cluster, where it is influenced by both fluctuating and secular terms. Since the systems under investigation are isolated pairs, $R_{0.9}$ is not directly comparable to the tidal radius of King's model.

We have tried to fit surface density profiles to the equilibrium models given in Table 3. Both Hubble's and de Vaucouleurs' laws have been tried, but the latter turns out to be the better fit. It has been shown by several workers that ellipticals and bulges of spiral galaxies can be well represented by de Vaucouleurs' law.

$$\log I(r) = \log I(0) - 3.33\left[\left(\frac{r}{r_{\rm e}}\right)^{1/4} - 1\right]. \qquad (7)$$

Here $r_{\rm e}$ is the radius that contains half the total light of the model and $I(0)$ is the brightness at $r_{\rm e}$. The simulated data have been fitted to the above law by the method of least squares. The fitted line and the data points are shown in Fig. 3. The profiles are displaced vertically for clarity. In each profile the solid line represents the best fit. The parameters of the best fit are given in columns 8 and 9 of Table 2. The formation of a core is observed in Figs 3(a)–(c). This phenomenon is not so pronounced in Fig. 3(d). Almost similar behaviour is exhibited in every model. The density structure is weakly dependent on the initial orbit and the structure of the galaxy. In Fig. 3(c), the slopes of the fitted lines are steeper than those of other models. The fit becomes better as the number of particles is increased.

Over the range in radii within which 90 per cent of the mass of the remnant system is situated, the density profiles of the initial and final configurations are remarkably similar. Departures from an $r^{1/4}$ law start at large distances from the centre, i.e. at $R > 4R_{\rm h}$, and therefore the possibility of observing this phenomenon is very remote. The radii of the final configuration in B models show maximum distension by a factor three times larger than the corresponding initial values. Loss of particles takes place from the outermost shells without causing significant changes in the inner regions. Departures in the outer parts become increasingly evident as the mass ratio decreases and approaches unity.

Earlier workers have noted the formation of a *bump* in the outer parts which disappeared gradually as the remnant approached an $r^{1/4}$ profile. Although this phenomenon has not been demonstrated convincingly, there is a tendency in our simulations to develop tidal distension in the outer parts of the density profiles of models P10 and E10 (mass ratio 2.6). Our results agree with Kormendy's (1977) suggestion

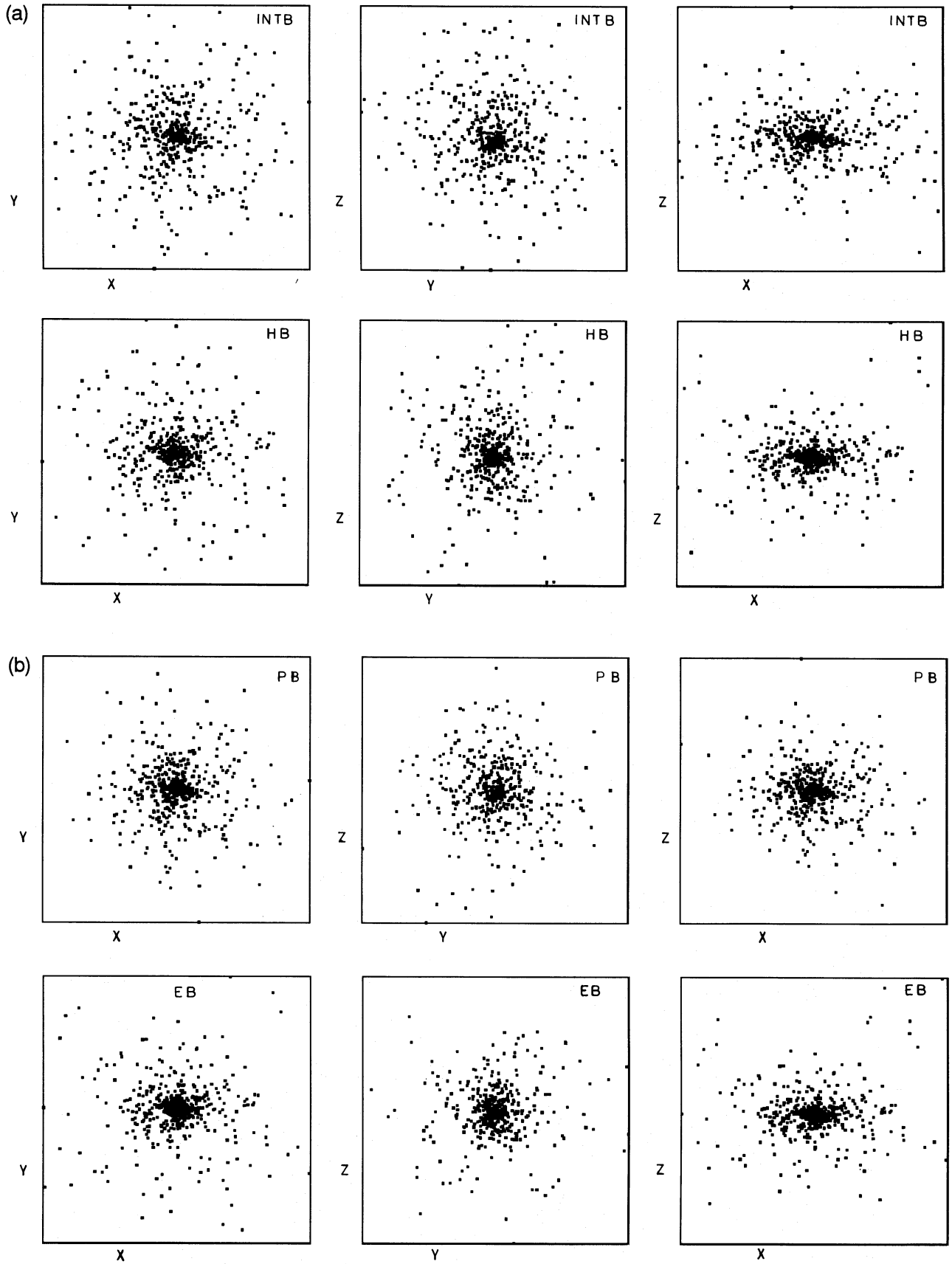

Figure 2. The projection of particles in the *XY, YZ* and *ZX* planes. (a) Initial model INTB (top) and model HB (bottom) after an encounter. (b) Model PB (top) and model EB (bottom) after an encounter. (c) Model INTC (top) and model HC (bottom) after an encounter. (d) Models PC (top) and EC (bottom) after an encounter.

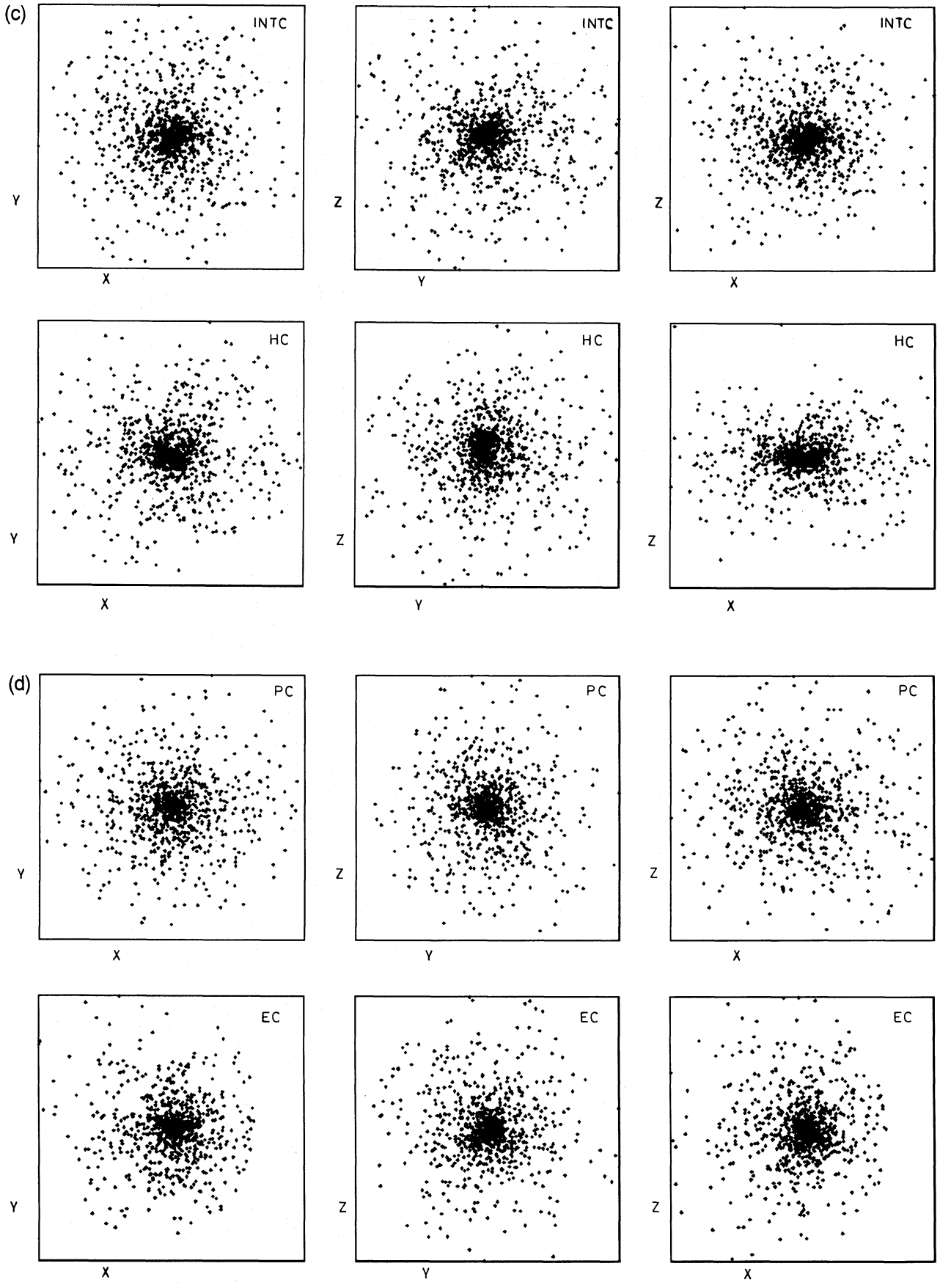

Figure 2 – *continued*

Table 3. Radial structure of remnant bound system for all models.

%	INT	H2	H3	H4	P4	P5	P6	P7	P8	P10	E5	E6	E7	E8	E10	C7	C8	C10	INTB	HB	PB	EB	INTC	HC	PC	EC
10	0.28	0.21	0.27	0.35	0.29	0.23	0.35	0.31	0.26	0.30	0.31	0.28	0.32	0.31	0.44	0.23	0.26	0.32	0.16	0.23	0.22	0.25	0.21	0.22	0.19	0.18
20	0.44	0.35	0.43	0.48	0.45	0.41	0.54	0.45	0.39	0.40	0.47	0.44	0.50	0.48	0.58	0.36	0.40	0.46	0.31	0.39	0.36	0.41	0.37	0.37	0.33	0.36
30	0.61	0.46	0.56	0.62	0.60	0.55	0.69	0.60	0.55	0.65	0.65	0.54	0.62	0.60	0.74	0.61	0.58	0.63	0.51	0.57	0.55	0.54	0.54	0.55	0.53	0.52
40	0.80	0.73	0.79	0.79	0.84	0.74	0.84	0.78	0.75	0.79	0.82	0.69	0.78	0.82	0.90	0.78	0.73	0.77	0.69	0.79	0.79	0.76	0.72	0.74	0.75	0.71
50	1.00	1.00	1.00	1.00	1.00	1.00	1.00	1.00	1.00	1.00	1.00	1.00	1.00	1.00	1.00	1.00	1.00	1.00	1.00	1.00	1.00	1.00	1.00	1.00	1.00	1.00
60	1.23	1.38	1.35	1.15	1.27	1.16	1.31	1.32	1.26	1.49	1.22	1.32	1.21	1.21	1.23	1.19	1.19	1.26	1.29	1.34	1.42	1.42	1.32	1.44	1.29	1.40
70	1.73	1.85	1.78	1.45	1.57	1.55	1.67	1.62	1.57	1.83	1.49	1.63	1.45	1.57	1.63	1.44	1.37	1.71	1.66	1.78	1.91	2.07	1.84	1.93	1.72	1.82
80	2.43	2.99	2.77	1.87	1.88	2.06	2.16	2.14	2.13	2.51	1.83	2.18	1.95	2.01	2.18	1.89	1.62	2.04	2.25	2.65	2.58	3.13	2.38	2.70	2.35	2.43
90	3.30	8.48	6.83	3.19	3.11	2.97	3.28	3.07	3.23	3.53	2.63	2.81	2.73	3.50	3.13	2.57	2.26	2.83	3.09	3.94	3.34	4.72	3.27	3.78	3.28	3.51
100	7.60	16.27	18.33	23.75	19.16	17.29	18.81	9.61	14.09	16.19	8.36	9.94	9.32	16.72	18.66	7.21	7.08	16.36	7.18	34.35	13.05	32.99	7.15	17.98	19.86	15.35
R_h	4.61	4.89	4.74	5.65	4.13	5.05	4.77	5.02	5.62	4.23	4.30	5.20	5.08	5.11	5.50	4.75	5.85	5.01	2.47	2.16	2.18	1.77	2.27	2.12	2.32	2.20
R_t		1.42	1.78	1.88	2.77	2.86	3.81	4.56	5.13	10.83	3.51	3.65	4.71	5.90	8.70	5.31	5.43	10.06		5.91	6.30	8.13		6.00	5.92	6.52

Note: R_h represents the half-mass radius and R_t, the tidal radius (expressed in units of R_h) as given by King's formula.

that mild encounters produce tidal distension of the outer parts of the galaxies. Furthermore, it has been observed that parabolic encounters in which the galaxies have comparable mass produce maximum tidal distension. White (1978) has shown that more particles escape from parabolically colliding systems than from those which are initially in bound orbits. McGlynn (1990) has noted that the presence of a steady tidal field in bound orbits produces less catastrophic effects than when the system is in non-bound orbits. This is due to the fact that the tidal forces are equal in magnitude and opposite in direction at diametrically opposite points in the orbit, as a result of which the tidal effects at these points cancel each other. Highly eccentric orbit encounters are not expected to produce significant rearrangements within the satellite. Moderately eccentric parabolic encounters are the ones which produce maximum tidal effects in the less massive companion. The encounter becomes more dramatic, culminating in the merger of the two stellar systems if they overlap each other when their separation is a minimum.

3.4 Comparison with previous work

An important conclusion of our simulations is that, in collisions of galaxies of unequal mass in which the pericentric distance is kept constant, the density profile of the remnant bound system can be fitted well with an $r^{1/4}$ law up to $r=4R_h$. Previous numerical studies by Aguilar & White (1986) used mass ratios in the range 0.4 to 6. They found that de Vaucouleurs' profile fits the final configuration even in very strong encounters which resulted in a mass loss as high as 50 per cent. No differences were observed between models with different internal orbital structures. The density profiles showed an extended tail after an encounter. These results are in good agreement with our results. The major difference between our results and the above is that we have used a wide range of values for the mass ratio and velocity of collision. Our results, therefore, are an extension of those of Aguilar & White to the case of weaker tidal encounters. In our simulations, the satellite galaxy suffers considerable damage if the mass loss exceeds 30 per cent. We have also noted that in such cases the fractional change in the energy, $\Delta U/|U|$, turns out to be greater than two, which can be considered as a necessary condition for tidal disruption (see Paper I).

McGlynn (1990) has shown that the density profiles of a shocked galaxy are well fitted with $\rho \propto r^{-4}$. He also noted the formation of a bulge in the tail of the profile, which he interpreted as due to the presence of nearly unbound particles. The bulge is expected to disappear when the models are allowed to evolve further. He used mass ratios 10^6 and 10^2. Our models have been evolved for sufficiently longer times to reach approximately stable systems, as can be inferred from the values of the virial coefficient q in Table 2. Consequently the bulges are not so prominent in our models as in the case of the models of the previous workers. However, there is evidence for a tendency to develop bulges in the outer parts in non-merging encounters in which the masses of the stellar systems are comparable. Detailed comparison with the above two works becomes difficult because our calculations either use a smaller number of particles or employ a different set of initial conditions.

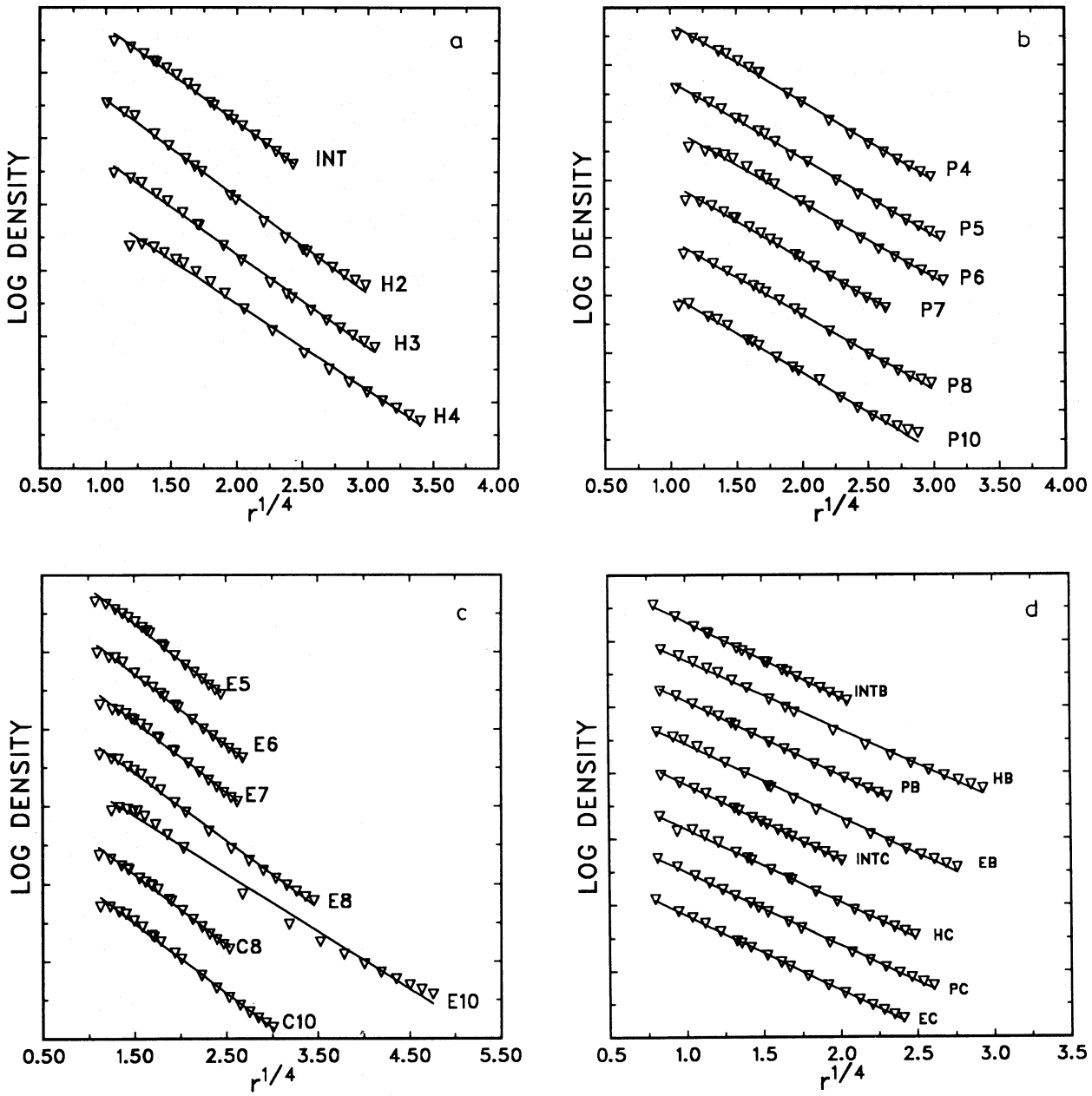

Figure 3. The surface density profiles of each model fitted with an $r^{1/4}$ profile. (a) Hyperbolic encounters of A model; INT is the profile of the initial system; (b) parabolc encounters of A model; (c) elliptic and circular encounters of A model; (d) B and C models; INTB and INTC respectively represent initial configurations of models B and C.

4 CONCLUSIONS

We have performed a series of numerical simulations of non-merging encounters of galaxies using various collision parameters like the mass ratio and the velocity of collision and also by varying the total number of particles in the galaxy. Our results are valid in the case of collisions of galaxies of unequal mass ($2 < M_1/M < 10^3$) in which the pericentric distance is kept constant and satisfies the condition $p > 3R$. It is quite remarkable that the half-mass radius of the remnant bound system remains nearly unaltered in all models. Hyperbolic encounters in A models show higher concentration towards the centre and expansion in the outer parts. In all other models, the region containing up to 90 per cent mass more or less remains unchanged; the outermost region containing the rest of the mass shows considerable expansion. Galaxies which are initially moving in parabolic orbits produce maximum tidal distension. The surface density profiles of the equilibrium systems closely follow an $r^{1/4}$ law. Deviations from this law start at large distances from the centre, i.e. at $r > 4R_h$, and the possibility of observing this phenomenon is very remote. The density structure of the remnant system is weakly dependent on the initial orbit and structure of the galaxy. The tendency to form tidally distended objects becomes increasingly evident as the mass ratio of the galaxies approaches unity.

ACKNOWLEDGMENTS

We thank Dr S. J. Aarseth for making available his NBODY code. We also thank an anonymous referee for useful suggestions and criticism.

REFERENCES

Aguilar L. A., White S. D. M., 1986, ApJ, 307, 97
Chandrasekhar S., 1943, ApJ, 97, 255
Dekel A., Lecar M., Shaham J., 1980, ApJ, 241, 946
Faber S. M., 1973, ApJ, 179, 423
Gelato S., Chernoff D. F., Wasserman I., 1992, ApJ, 384, 15
Gutowski W. J., Larson R. B., 1976, PASP, 88, 374
King I. R., 1962, AJ, 67, 471
Kormendy J., 1977, ApJ, 218, 333
McGlynn T. A., 1990, ApJ, 348, 515
Miller R. H., Smith B. F., 1980, ApJ, 235, 421
Namboodiri P. M. S., Kochhar R. K., 1990, MNRAS, 243, 276 (Paper I)
Navarro J. F., 1989, MNRAS, 239, 257
Navarro J. F., 1990, MNRAS, 242, 311
Nieto J.-L., Prugniel P., 1987, in de Zeeuw T., ed., Structure and Dynamics of Elliptical Galaxies. Reidel, Dordrecht, p. 99
Prugniel P., Davoust E., Nieto J.-L., 1989, A&A, 222, 5
Rao P. D., Ramamani N., Alladin S. M., 1987, JA&A, 8, 17
Tremaine S., Weinberg M. D., 1984, MNRAS, 209, 729
van Albada T. S., van Gorkom J. H., 1977, A&A, 54, 121
White S. D. M., 1978, MNRAS, 184, 185
White S. D. M., 1979, MNRAS, 189, 831
Wielen R., 1977, in Tinsley B. M., Larson R. B., eds, The Evolution of Galaxies and Stellar Populations. Yale Univ. Observatory, p. 397